



Hygrothermal coupling analysis of magneto-electroelastic beams using finite element methods

M. Vinyas, Subhas Chandra Kattimani & Sharnappa Joladarashi

To cite this article: M. Vinyas, Subhas Chandra Kattimani & Sharnappa Joladarashi (2018) Hygrothermal coupling analysis of magneto-electroelastic beams using finite element methods, Journal of Thermal Stresses, 41:8, 1063-1079, DOI: [10.1080/01495739.2018.1447856](https://doi.org/10.1080/01495739.2018.1447856)

To link to this article: <https://doi.org/10.1080/01495739.2018.1447856>



Published online: 29 Mar 2018.



Submit your article to this journal [↗](#)




Article views: 79



View Crossmark data [↗](#)



Hygrothermal coupling analysis of magneto-electroelastic beams using finite element methods

M. Vinyas, Subhas Chandra Kattimani , and Sharnappa Joladarashi

Department of Mechanical Engineering, National Institute of Technology Karnataka, Surathkal, Mangalore, India

ABSTRACT

In this article, the finite element (FE) method has been used to assess the coupled static behavior of hygro-thermo-magneto-electroelastic (HTMEE) beam. Influence of externally applied hygrothermal loads on the direct (displacements, electric and magnetic potentials) and derived quantities (stresses, electric displacement and magnetic flux densities) of HTMEE beam have been studied in detail. The principle of total potential energy and the coupled constitutive equations of HTMEE material are used for the FE formulation. A generalized condensation technique is adopted to solve the global FE equations of motion. Numerical examples are discussed to examine the effect of hygrothermal loads and distinct effect of moisture concentration on the behavior of the beam. Particular emphasis has been placed to analyze the influence of temperature and moisture dependent elastic stiffness coefficients associated with empirical constants. Considering the independent effect of temperature and moisture on the coupled static responses, the most significant combination of the empirical constants corresponding to temperature dependency and moisture dependency are explored. Extensive computational examples are considered to examine the significant effect of boundary conditions, temperature gradient, moisture concentration gradient and empirical constants on the static behavior of HTMEE beam. It is observed that the static behavior of HTMEE beam is significantly influenced by the hygrothermal loads and empirical constants. The results presented in this article would serve as a benchmark results in design and analysis of HTMEE structures for sensors and actuators applications.

ARTICLE HISTORY



Received 13 January 2018
Accepted 28 February 2018

KEYWORDS

Empirical constants; finite element methods; hygrothermo-magneto-electroelastic; moisture concentration; multiphysics coupling

Introduction

In recent years, noticeable efforts are being made to achieve the possible advantages of the various coupled behavior of piezoelectric, piezomagnetic, and magneto-electroelastic (MEE) materials. Among them, analysis of MEE structures is recognized as an intensive and revolutionary research field. This material exhibits coupling between elastic, magnetic and electric field which is not noticed in the monolithic material. This unique, multifunctional ability and potential property of MEE materials make it convenient to adopt in smart structural applications such as sensors, actuators, energy harvesters, aeronautics, micro-electromechanical systems, smart structural engineering etc. During the operation, MEE structures are often exposed to diverse conditions of temperature and humidity. As a result the MEE materials become more sensitive and exhibit additional thermoelectric and thermomagnetic coupling which is termed as a pyroelectric and pyromagnetic effect, respectively. These coupling effects diminish the performance of MEE structures. Hence, the analysis of MEE structures under these harsh environments is an area of concern.

CONTACT Subhas Chandra Kattimani  sck@nitk.ac.in  Department of Mechanical Engineering, National Institute of Technology Karnataka, Surathkal, Srinivasnagar Post, Mangalore 575025, India.

Color versions of one or more of the figures in the article can be found online at www.tandfonline.com/uths.

The coupling among the elastic, electric, magnetic, thermal and hygroscopic fields influence the sensing and actuation properties of smart materials [1, 2]. Considerable research work has been devoted on evaluating the structural behavior of piezoelectric smart structures under hygrothermal condition [3–7]. Kerur and Ghosh [8] considered the hygro-thermo-electroelastic coupled problem and developed an finite element (FE) formulation to assess the geometrically nonlinear bending behavior of smart structures. Using the variational principles, Altay and Dokmeci [9] analyzed the fundamental equations of piezoelectric, thermopiezoelectric and hygro-thermopiezoelectric materials.

By virtue of increased demand of the smart materials, the analysis of intelligent structures made of MEE materials have been a great interest. The various computational techniques such as analytical method, exact solution method, state vector approach etc., have been developed to evaluate the free vibration characteristics [10–14], static behavior [15–19] and buckling behavior [20, 21] of MEE structures. Nonlinear vibration control of MEE plates and shells using active constrained layer damping treatment has been studied by Kattimani and Ray [22, 23] by considering the different stacking sequence and boundary conditions. They extended their analysis to the functionally graded MEE plates also [24].

The behavior of MEE structures exposed to thermal loading is a prominent issue and a remarkable attention is being paid in the recent years. Sunar [25] demonstrated the coupled behavior of a thermopiezomagnetic continuum using a FE formulation. Ootao and Tanigawa [26] developed an exact solution for the transient behavior of multilayered magneto-electro-thermoelastic (METE) strip subjected to nonuniform and unsteady heating. They also studied the effect of different forms of thermal loading. Kumaravel et al. [27, 28] evaluated the effect of thermal loads, stacking sequence and boundary conditions on the static behavior of MEE beam. They extended their evaluation to predict the buckling behavior of layered and multiphase MEE beams under thermal environment. Further, in the presence of thermal environment, MEE materials exhibit an additional coupling between thermoelectric and thermomagnetic fields. This leads to the development of pyroloads which significantly affects the behavior of MEE structures. The influence of pyroelectric and pyromagnetic coupling on the direct and derived quantities of MEE structures (beams, plates, and shells) has been investigated by Kondaiah et al. [29, 30]. Vinyas and Kattimani [31–33] proposed an FE formulation to analyze the effect of different thermal loads on the static behavior of stepped functionally graded (SFG) and multiphase MEE plates and beams. They extended the FE study for hygrothermal analysis of MEE plates [34]. In addition, Vinyas and Kattimani [35] presented a fully coupled FE formulation to assess the static behavior of SFG-METE plates under various forms of loading. More recently, they evaluated the effect of different particle arrangement of MEE composites on the static response of METE plates [36].

The multiphysics response of MEE structures under the influence of humidity and temperature loads has been investigated by a limited number of researchers. In an effort to analyze the coupled HTMEE response, the first attempt was made by Akbarzadeh and Chen [37]. They considered the temperature and moisture dependent material properties and computed the influence of hygrothermal loads on MEE behavior of rotating cylinders. They also proposed an analytical solution to estimate the hygrothermal stresses developed in one-dimensional FG piezoelectric media [38]. Akbarzadeh and Pasini [39] derived closed-form solutions to examine the effect of hygrothermal loading on the steady state responses of FG infinitely long cylinders and thin circular disks. Saadatfar and Khafri [40] evaluated the coupled hygro-thermo-magneto-electroelastic (HTMEE) response of FG-MEE hollow sphere resting on elastic foundation.

The comprehensive literature review reveals that an inadequate research has been reported on HTMEE response of MEE structures. To the best of authors' knowledge, the FE study dealing with the static analysis of HTMEE beams subjected to hygrothermal loading are not found in open literature. Hence, the present article makes the first attempt to develop an FE formulation to evaluate the coupled multiphysics response of HTMEE beams. In addition, the influences of the temperature and moisture dependent elastic coefficients are studied through the empirical constants.

Basic formulation of the problem

Problem description

Figure 1 depicts the schematic representation of an adaptive wood HTMEE beam composed of barium titanate (BaTiO_3) and cobalt ferric oxide (CoFe_2O_4). The length a , width w , and thickness h , are considered along the x , y , and z -axes of the coordinate system, respectively, as shown in Figure 1. It is assumed that the HTMEE beam is exposed to a hygrothermal environment which corresponds to a temperature rise of ΔT and humidity concentration variation of Δm .

Constitutive equations

The linear coupled constitutive equations of an HTMEE material can be written as follows:

$$\{\sigma\} = [C]\{\varepsilon\} - [e]\{E\} - [q]\{H\} - [C] (\{\alpha\}\Delta T - \{\xi\}\Delta m) \tag{1}$$

$$\{D\} = [e]^T\{\varepsilon\} + [\eta]\{E\} + [m]\{H\} + \{p\}\Delta T + \{\chi\}\Delta m \tag{2}$$

$$\{B\} = [q]^T\{\varepsilon\} + [m]\{E\} + [\mu]\{H\} + \{\tau\}\Delta T + \{\nu\}\Delta m \tag{3}$$

in which, the term $[C] \{\alpha\} \Delta T$ is the thermal stress developed due to temperature gradient ΔT , $[C] \{\xi\} \Delta m$ corresponds to the hygroscopic stresses generated as a result of moisture concentration gradient Δm ; $[C]$, $[e]$, $[q]$, $\{\alpha\}$ and $\{\xi\}$ are the elastic coefficient matrix, piezoelectric coefficient matrix, magnetostrictive coefficient matrix, thermal expansion coefficient vector, and moisture expansion coefficient vector, respectively; $[\eta]$, $[m]$, $\{p\}$, $\{\tau\}$, $[\mu]$, $\{\chi\}$, and $\{\nu\}$ represent the dielectric constant matrix, electromagnetic coefficient matrix, pyroelectric coefficient vector, pyromagnetic coefficient vector, magnetic permeability constant matrix, hygroelectric coefficient vector, and hygromagnetic coefficient vector, respectively; $\{\sigma\}$, $\{D\}$, and $\{B\}$ indicate the stress tensor, electric displacement vector and the magnetic flux vector, respectively; $\{\varepsilon\}$, $\{E\}$, $\{H\}$ are the linear strain tensor, electric field vector, magnetic field vector, respectively.

Finite element formulation

A FE model of the HTMEE beam is developed using an eight noded 3D isoparametric brick element. The entire beam structure is discretized into 10 elements. Five degrees of freedom are considered at each node of the element which corresponds to three translational displacement fields, one electric potential field (ϕ) and one magnetic potential (ψ) field. The generalized translational displacement vector associated with the i th ($i = 1, 2, 3, \dots, 8$) node of the element can be expressed as

$$\{d_{ti}\} = [U_x U_y U_w]^T \tag{4}$$

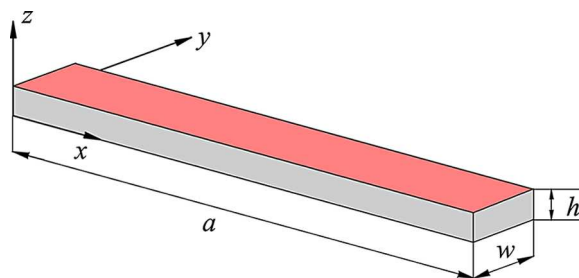


Figure 1. Schematic representation of HTMEE beam. Note: HTMEE, hygro-thermo-magneto-electroelastic.

The generalized displacement vector $\{d_t\}$, electric potential vector $\{\phi\}$, and magnetic potential vector $\{\psi\}$ can be represented with regard to the nodal displacement vector $\{d_t^e\}$, the nodal electric potential vector $\{\phi^e\}$, and the nodal magnetic potential vector $\{\psi^e\}$, respectively, as follows:

$$\{d_t\} = [N_t] \{d_t^e\}, \{\phi\} = [N_\phi] \{\phi^e\}, \{\psi\} = [N_\psi] \{\psi^e\} \tag{5}$$

The nodal displacement vector $\{d_t^e\}$, nodal electric potential vector $\{\phi^e\}$, and the nodal magnetic potential vector $\{\psi^e\}$ appearing in Eq. (5) may be expressed as follows:

$$\{d_t^e\} = [\{d_{t1}\}^T \{d_{t2}\}^T \dots \{d_{t8}\}^T]^T, \{\phi^e\} = [\phi_1 \phi_2 \dots \phi_8]^T, \{\psi^e\} = [\psi_1 \psi_2 \dots \psi_8]^T \tag{6}$$

The various shape function matrices ($[N_t]$, $[N_\phi]$, and $[N_\psi]$) appearing in Eq. (5) are described as

$$[N_t] = [N_{t1}N_{t2} \dots N_{t8}], N_{ti} = N_i I_t, [N_\phi] = [N_\psi] = [N_1N_2 \dots N_8] \tag{7}$$

where N_i is the natural coordinate shape function associated with the i th node of the element; I_t is the identity matrix. The shape functions for the eight noded isoparametric brick element in the natural coordinate (ξ, η, ζ) are given by

$$N_i(\xi, \eta, \zeta) = \frac{1}{8} (1 + \xi\xi_i) (1 + \eta\eta_i) (1 + \zeta\zeta_i); \quad i = 1, 2, 3, \dots, 8 \tag{8}$$

The relation between the electric intensity (E) and electric potential (ϕ); magnetic intensity (H); and magnetic potential (ψ) can be established using Maxwell's equations as follows:

$$E_x = -\frac{\partial\phi}{\partial x}; E_y = -\frac{\partial\phi}{\partial y}; E_z = -\frac{\partial\phi}{\partial z} \tag{9}$$

$$H_x = -\frac{\partial\psi}{\partial x}; H_y = -\frac{\partial\psi}{\partial y}; H_z = -\frac{\partial\psi}{\partial z} \tag{10}$$

With the aid of the derivative of shape function matrices $[B_t]$, $[B_\phi]$, and $[B_\psi]$ and the nodal elemental vectors $\{d_t^e\}$, $\{\phi^e\}$, and $\{\psi^e\}$, the derived field vectors such as strain vector $\{\varepsilon\}$, electric intensity $\{E\}$, and magnetic intensity vector $\{H\}$ of the HTMEE beam can be written as follows:

$$\{\varepsilon\} = [B_t] \{d_t^e\}; \{E\} = [B_\phi] \{\phi^e\}, \{H\} = [B_\psi] \{\psi^e\} \tag{11}$$

The shape function derivative matrices appearing in Eq. (11) can be written as

$$[B_t] = [B_{t1}B_{t2} \dots B_{t8}], [B_\psi] = [B_{\psi 1}B_{\psi 2} \dots B_{\psi 8}], [B_\phi] = [B_{\phi 1}B_{\phi 2} \dots B_{\phi 8}] \tag{12}$$

in which, the submatrices, $[B_{ti}]$, $[B_{\psi i}]$, and $[B_{\phi i}]$ are given by

$$[B_{ti}] = \begin{bmatrix} \frac{\partial N_i}{\partial x} & 0 & 0 \\ 0 & \frac{\partial N_i}{\partial y} & 0 \\ 0 & 0 & \frac{\partial N_i}{\partial z} \\ 0 & \frac{\partial N_i}{\partial z} & \frac{\partial N_i}{\partial y} \\ \frac{\partial N_i}{\partial z} & 0 & \frac{\partial N_i}{\partial x} \\ \frac{\partial N_i}{\partial y} & \frac{\partial N_i}{\partial x} & 0 \end{bmatrix}, [B_{\psi i}] = \begin{bmatrix} -\frac{\partial N_i}{\partial x} \\ -\frac{\partial N_i}{\partial y} \\ -\frac{\partial N_i}{\partial z} \end{bmatrix}, [B_{\phi i}] = \begin{bmatrix} -\frac{\partial N_i}{\partial x} \\ -\frac{\partial N_i}{\partial y} \\ -\frac{\partial N_i}{\partial z} \end{bmatrix} \tag{13}$$

where $i = 1, 2, 3, \dots, 8$ represents the node number.

Finite element equations of motion

The principle of total potential energy along with the constitutive equations of HTMEE material are utilized to derive the governing equations of motion. Further, the total potential energy is minimized as follows [34]:

$$T_p = \frac{1}{2} \left[\int_{\Omega} \delta \{ \varepsilon \}^T \{ \sigma \} d\Omega - \int_{\Omega} \delta \{ E \}^T \{ D \} d\Omega - \int_{\Omega} \delta \{ H \}^T \{ B \} d\Omega \right] - \int_A \delta \{ d_t \}^T \{ f \} dA - \int_A \delta \{ \phi \} Q^\phi dA - \int_A \delta \{ \psi \} Q^\psi dA = 0 \tag{14}$$

where $\{ f \}$ is the traction force vector acting over an area A . The entire volume of the domain is represented by Ω . The surface electric charge density and surface magnetic charge density are denoted by Q^ϕ and Q^ψ , respectively.

Substituting Eqs. (1)–(3) into Eq. (14), we get,

$$T_p = \frac{1}{2} \int_{\Omega} \delta \{ \varepsilon \}^T [C] \{ \varepsilon \} d\Omega - \frac{1}{2} \int_{\Omega} \delta \{ \varepsilon \}^T [e] \{ E \} d\Omega - \frac{1}{2} \int_{\Omega} \delta \{ \varepsilon \}^T [q] \{ H \} d\Omega - \frac{1}{2} \int_{\Omega} \delta \{ \varepsilon \}^T [C] \{ \alpha \} \Delta T d\Omega - \frac{1}{2} \int_{\Omega} \delta \{ \varepsilon \}^T [C] \{ \xi \} \Delta m d\Omega - \frac{1}{2} \int_{\Omega} \delta \{ E \}^T [e]^T \{ \varepsilon \} d\Omega - \frac{1}{2} \int_{\Omega} \delta \{ E \}^T [\eta]^T \{ E \} d\Omega - \frac{1}{2} \int_{\Omega} \delta \{ E \}^T [m]^T \{ H \} d\Omega - \frac{1}{2} \int_{\Omega} \delta \{ E \}^T \{ p \} \Delta T d\Omega - \frac{1}{2} \int_{\Omega} \delta \{ E \}^T \{ \chi \} \Delta m d\Omega - \frac{1}{2} \int_{\Omega} \delta \{ H \}^T [q]^T \{ \varepsilon \} d\Omega - \frac{1}{2} \int_{\Omega} \delta \{ H \}^T [m] \{ E \} d\Omega - \frac{1}{2} \int_{\Omega} \delta \{ H \}^T [\mu] \{ H \} d\Omega - \frac{1}{2} \int_{\Omega} \delta \{ H \}^T \{ \tau \} \Delta T d\Omega - \frac{1}{2} \int_{\Omega} \delta \{ H \}^T \{ \nu \} \Delta m d\Omega - \int_A \delta \{ d_t \}^T \{ f \} dA - \int_A \delta \{ \phi \} Q^\phi dA - \int_A \delta \{ \psi \} Q^\psi dA = 0 \tag{15}$$

Meanwhile, Eqs. (5), (7), (8), and (11) are substituted in Eq. (15) to obtain

$$T_p = \frac{1}{2} \int_{\Omega} \delta \{ d_t^e \}^T [B_t]^T [C] [B_t] \{ d_t^e \} d\Omega - \frac{1}{2} \int_{\Omega} \delta \{ d_t^e \}^T [B_t]^T [e] [B_\phi] \{ \phi^e \} d\Omega - \frac{1}{2} \int_{\Omega} \delta \{ d_t^e \}^T [B_t]^T [q] [B_\psi] \{ \psi^e \} d\Omega - \frac{1}{2} \int_{\Omega} \delta \{ d_t^e \}^T [B_t]^T [C] \{ \alpha \} \Delta T d\Omega - \frac{1}{2} \int_{\Omega} \delta \{ d_t^e \}^T [B_t]^T [C] \{ \xi \} \Delta m d\Omega - \frac{1}{2} \int_{\Omega} \delta \{ \phi^e \}^T [B_\phi]^T [e]^T [B_t] \{ d_t^e \} d\Omega - \frac{1}{2} \int_{\Omega} \delta \{ \phi^e \}^T [B_\phi]^T [\eta] [B_\phi] \{ \phi^e \} d\Omega - \frac{1}{2} \int_{\Omega} \delta \{ \phi^e \}^T [B_\phi]^T [m] [B_\psi] \{ \psi^e \} d\Omega - \frac{1}{2} \int_{\Omega} \delta \{ \phi^e \}^T [B_\phi]^T \{ p \} \Delta T d\Omega - \frac{1}{2} \int_{\Omega} \delta \{ \phi^e \}^T [B_\phi]^T \{ \chi \} \Delta m d\Omega - \frac{1}{2} \int_{\Omega} \delta \{ \psi^e \}^T [B_\psi]^T [q]^T [B_t] \{ d_t^e \} d\Omega - \frac{1}{2} \int_{\Omega} \delta \{ \psi^e \}^T [B_\psi]^T [m] [B_\phi] \{ \phi^e \} d\Omega - \frac{1}{2} \int_{\Omega} \delta \{ \psi^e \}^T [B_\psi]^T [\mu] [B_\psi] \{ \psi^e \} d\Omega - \frac{1}{2} \int_{\Omega} \delta \{ \psi^e \}^T [B_\psi]^T \{ \tau \} \Delta T d\Omega$$

$$\begin{aligned}
 & -\frac{1}{2} \int_{\Omega} \delta \{ \psi^e \}^T [B_{\psi}]^T \{ v \} \Delta m \, d\Omega^e - \int_A \delta \{ d_t^e \}^T [N_t]^T \{ f^e \} \, dA \\
 & - \int_A \delta \{ \phi^e \} [N_{\phi}] Q^{\phi} \, dA - \int_A \delta \{ \psi^e \} [N_{\psi}] Q^{\psi} \, dA = 0
 \end{aligned} \tag{16}$$

Assigning stiffness matrices to various terms, Eq. (16) can be rewritten as

$$\begin{aligned}
 T_p^e &= \int_{\Omega} \delta \{ d_t^e \}^T [K_{tt}^e] \{ d_t^e \} \, d\Omega^e - \int_{\Omega} \delta \{ d_t^e \}^T [K_{t\phi}^e] \{ \phi^e \} \, d\Omega^e - \int_{\Omega} \delta \{ d_t^e \}^T [K_{t\psi}^e] \{ \psi^e \} \, d\Omega^e \\
 & - \int_{\Omega} \delta \{ d_t^e \}^T \{ F_{th}^e \} \, d\Omega^e - \int_{\Omega} \delta \{ d_t^e \}^T \{ F_{hy}^e \} \, d\Omega^e - \int_{\Omega} \delta \{ \phi^e \}^T [K_{t\phi}^e]^T \{ d_t^e \} \, d\Omega^e \\
 & - \int_{\Omega} \delta \{ \phi^e \}^T [K_{\phi\phi}^e] \{ \phi^e \} \, d\Omega^e - \int_{\Omega} \delta \{ \phi^e \}^T [K_{\phi\psi}^e] \{ \psi^e \} \, d\Omega^e \\
 & - \int_{\Omega} \delta \{ \phi^e \}^T \{ F_{p,e}^e \} \, d\Omega^e - \int_{\Omega} \delta \{ \phi^e \}^T \{ F_{h,e}^e \} \, d\Omega^e - \int_{\Omega} \delta \{ \psi^e \}^T [K_{t\psi}^e]^T \{ d_t^e \} \, d\Omega^e \\
 & - \int_{\Omega} \delta \{ \psi^e \}^T [K_{\phi\psi}^e]^T \{ \phi^e \} \, d\Omega^e - \int_{\Omega} \delta \{ \psi^e \}^T [K_{\psi\psi}^e] \{ \psi^e \} \, d\Omega^e \\
 & - \int_{\Omega} \delta \{ \psi^e \}^T \{ F_{p,m}^e \} \, d\Omega^e - \int_{\Omega} \delta \{ \psi^e \}^T \{ F_{h,m}^e \} \, d\Omega^e - \int_A \delta \{ d_t^e \}^T [N_t]^T \{ f^e \} \, dA \\
 & - \int_A \delta \{ \phi^e \} \{ F_{\phi}^e \} \, dA - \int_A \delta \{ \psi^e \} \{ F_{\psi}^e \} \, dA = 0
 \end{aligned} \tag{17}$$

in which, $[K_{tt}^e]$, $[K_{\phi\phi}^e]$, $[K_{\psi\psi}^e]$, $[K_{t\phi}^e]$, $[K_{t\psi}^e]$, and $[K_{\phi\psi}^e]$ are the elemental coupled stiffness matrices corresponding to elastic, electric, magnetic, electroelastic, magnetoelastic, and electromagnetic fields, respectively. Similarly, $\{ F_m^e \}$, $\{ F_{th}^e \}$, $\{ F_{hy}^e \}$, $\{ F_{h,e}^e \}$, $\{ F_{h,m}^e \}$, $\{ F_{\phi}^e \}$, $\{ F_{\psi}^e \}$, $\{ F_{p,e}^e \}$, and $\{ F_{p,m}^e \}$ are the elemental mechanical load vector, thermal load vector, hygroscopic load vector, hygroelectric load vector, hygomagnetic load vector, electric charge load vector, magnetic current load vector, pyroelectric load vector, and pyromagnetic load vector, respectively. The explicit forms of these matrices and load vectors can be written as follows:

$$[K_{tt}^e] = \int_{\Omega} [B_t]^T [C] [B_t] \, d\Omega^e,$$

$$[K_{t\phi}^e] = \int_{\Omega} [B_t]^T [e] [B_{\phi}] \, d\Omega^e [K_{t\psi}^e] = \int_{\Omega} [B_t]^T [q] [B_{\psi}] \, d\Omega^e [K_{\phi\phi}^e] = \int_{\Omega} [B_{\phi}]^T [\eta] [B_{\phi}] \, d\Omega^e,$$

$$[K_{\phi\psi}^e] = \int_{\Omega} [B_{\phi}]^T [m] [B_{\psi}] \, d\Omega^e, [K_{\psi\psi}^e] = \int_{\Omega} [B_{\psi}]^T [\mu] [B_{\psi}] \, d\Omega^e$$

$$\{ F_m^e \} = \int_A [N_t]^T f \, dA, \{ F_{\phi}^e \} = \int_A [N_{\phi}]^T Q^{\phi} \, dA, \{ F_{\psi}^e \} = \int_A [N_{\psi}]^T Q^{\psi} \, dA,$$

$$\{ F_{th}^e \} = \int_{\Omega} [B_t]^T [C] \{ \alpha \} \Delta T \, d\Omega^e, \{ F_{hy}^e \} = \int_{\Omega} [B_t]^T [C] \{ \xi \} \Delta m \, d\Omega^e$$

$$\begin{aligned} \{F_{p,e}^e\} &= \int_{\Omega} [B_{\phi}]^T \{p\} \Delta T d\Omega^e, \{F_{p,m}^e\} = \int_{\Omega} [B_{\psi}]^T \{\tau\} \Delta T d\Omega^e, \\ \{F_{h,m}^e\} &= \int_{\Omega} [B_{\psi}]^T \{v\} \Delta m d\Omega^e, \{F_{h,e}^e\} = \int_{\Omega} [B_{\phi}]^T \{\chi\} \Delta m d\Omega^e \end{aligned} \tag{18}$$

To develop the equilibrium equations, the terms associated with the coefficients of $\{d_t^e\}^T$, $\{\phi^e\}^T$, and $\{\psi^e\}^T$ are grouped together for the ease of simplification. Further, neglecting the mechanical load $\{F_m^e\}$, the elemental electric charge load $\{F_{\phi}^e\}$ and elemental magnetic current $\{F_{\psi}^e\}$, the elemental equations of motion are globalized in a straight forward manner to obtain the global equations of motion as follows:

$$[K_{tt}^g] \{d_t\} + [K_{t\phi}^g] \{\phi\} + [K_{t\psi}^g] \{\psi\} = \{F_{th}^g\} + \{F_{hy}^g\} \tag{19}$$

$$[K_{t\phi}^g]^T \{d_t\} - [K_{\phi\phi}^g] \{\phi\} - [K_{\phi\psi}^g] \{\psi\} = \{F_{p,e}^g\} + \{F_{h,e}^g\} \tag{20}$$

$$[K_{t\psi}^g]^T \{d_t\} - [K_{\phi\psi}^g]^T \{\phi\} - [K_{\psi\psi}^g] \{\psi\} = \{F_{p,m}^g\} + \{F_{h,m}^g\} \tag{21}$$

where the superscript *g* represents the globalized value of the corresponding stiffness matrices and force vectors. Using condensation approach, Eqs. (19)–(21) are solved to compute the displacement vector due to external hygrothermal loads. Thereafter, the obtained displacement vectors are used to determine the electric potential vector and magnetic potential vector. From the constitutive equations, the postcomputation procedure is performed to estimate the remaining fields viz. $\{\sigma\}$, $\{D\}$, and $\{B\}$. The detailed condensation technique used is described in [Appendix A](#). Consequently the final equilibrium equation can be expressed as

$$[K_{eq}] \{d_t\} = \{F_{eq}\} \tag{22}$$

where $[K_{eq}]$ and $\{F_{eq}\}$ are the equivalent stiffness matrix and force vector, respectively.

Results and discussion

This section addresses the credibility of the proposed FE formulation in predicting the static behavior of HTMEE beam subjected to moisture and temperature loads. Numerical calculations are performed using the FE formulation derived in the earlier section. However, to the best of authors’ knowledge, no work has been reported on static studies of MEE beams in hygrothermal environment. Hence, in the present study, the FE formulation is validated neglecting the hygroscopic effect. The numerical study considered by Kondaiah et al. [29] is solved using the present FE formulation. A comparative study is performed to justify the correctness of the proposed FE model. The results depicted in [Figure 2a, b](#) reveal that the present FE formulation closely agrees with Kondaiah et al. [29]. The independent effect of moisture concentration gradient, temperature and moisture dependent material properties, empirical constants and boundary conditions on the static behavior of HTMEE beam is demonstrated. The geometrical dimensions of the HTMEE beam is assumed as follows: length (*a*) = 1 m, width (*w*) = 0.1 m, and thickness (*h*) = 0.1 m. In the present analysis, the material properties of adaptive wood made of barium titanate (BaTiO₃) and cobalt ferric oxide (CoFe₂O₄) tabulated in [Table 1](#) are considered. The mesh size of 10 × 10 × 12 elements shows better convergence. Hence the same is used in the present analysis.

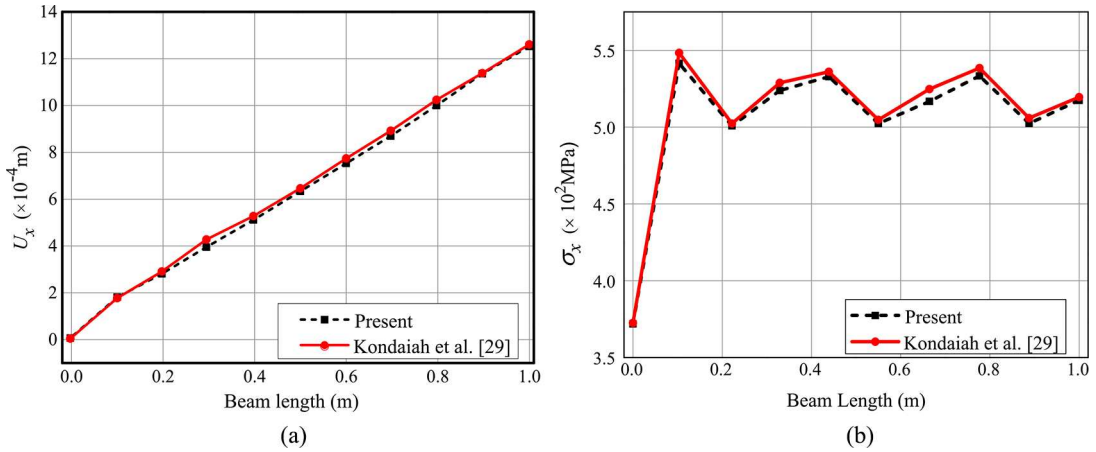


Figure 2. Validation plots (a) x-direction displacement component, U_x (b) normal stress σ_x .

Table 1. Material properties of adaptive wood made of BaTiO₃ and CoFe₂O₄ (Akbarzadeh and Chen [37]; Kondaiah et al. [29]; Vinyas and Kattimani [31]).

Material property	Material constants	Adaptive wood
Elastic constants (GPa)	$C_{11} = C_{22}$	286
	C_{12}	173
	$C_{13} = C_{23}$	170.5
	C_{33}	269.5
	$C_{44} = C_{55}$	45.3
	C_{66}	56.5
Piezoelectric constants ($C\ m^{-2}$)	e_{31}	-4.4
	e_{33}	18.6
	e_{15}	11.6
Dielectric constant ($10^{-9}\ C^2\ Nm^{-2}$)	$\epsilon_{11} = \epsilon_{22}$	0.08
	ϵ_{33}	0.093
Magnetic permeability ($10^{-4}\ Ns^2\ C^{-2}$)	$\mu_{11} = \mu_{22}$	-5.9
	μ_{33}	1.57
Piezomagnetic constants ($N\ Am^{-1}$)	q_{31}	580
	q_{33}	700
	q_{15}	560
	$m_{11} = m_{22}$	0
Magnetolectric constant ($10^{-12}\ Ns\ VC^{-1}$)	m_{33}	3
	p_2	-13
Pyroelectric constant ($10^{-5}\ C\ m^{-2}\ K^{-1}$)	τ_2	6
Pyromagnetic constant ($10^{-3}\ C\ m^{-2}\ K^{-1}$)	$\alpha_1 = \alpha_2$	14.1
Thermal expansion coefficient ($10^{-6}\ K^{-1}$)	α_3	7.2
	β_1	0
Moisture expansion coefficient ($\times 10^{-4}\ m^3\ kg^{-1}$)	$\beta_2 = \beta_3$	1.1
	ρ	5,300
Density ($kg\ m^{-3}$)		

Effect of hygrothermal loads

The influence of uniform hygrothermal loads of different magnitude on the direct (displacements, electric potential, and magnetic potential) and derived quantities (stresses, electric displacements and magnetic flux densities) of clamped-clamped (C-C) HTMEE beam are evaluated. Figure 3a-e illustrate the effect of hygrothermal loads on the static quantities of C-C HTMEE beam. The direct and derived quantities increase with the increase in hygrothermal loads in accordance with Eq. (22). For the sake of brevity, only prominent static parameters are illustrated. The undulating effect of ϕ and ψ (Figure 3a, b)

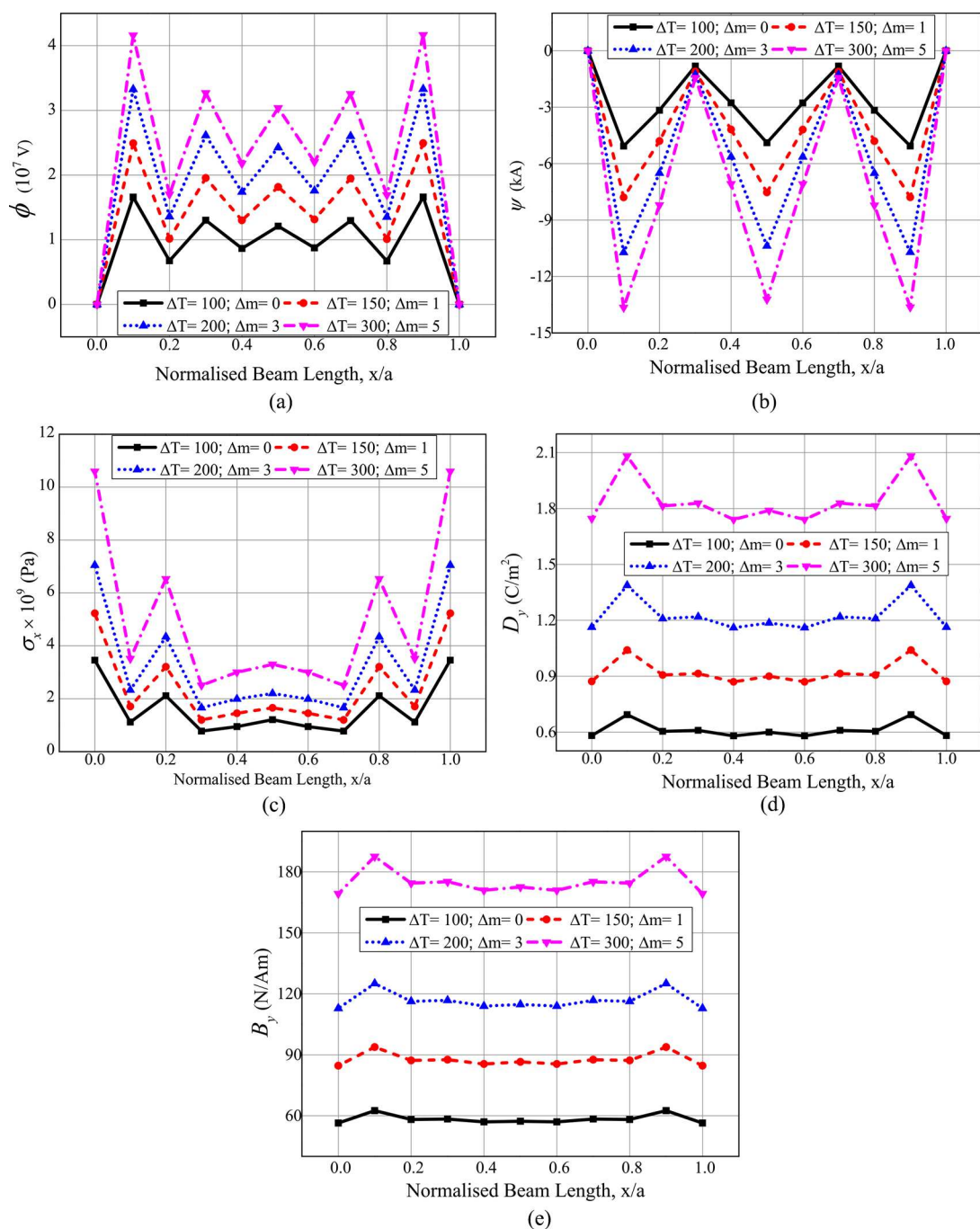


Figure 3. Effect of hygrothermal loads on (a) electric potential ϕ , (b) magnetic potential ψ , (c) normal stress σ_x , (d) electric displacement D_y , and (e) magnetic flux density component B_y for C–C HTMEE beam. Note: HTMEE, hygro-thermo-magneto-electroelastic.

can be attributed to the varying degree of coupling along the beam length due to the influence of pyroeffects. Moreover, at the clamped end, the pyroeffects display more prominent effect [29, 33]. Hence, a sudden rise in the value of these parameters is witnessed at the clamped end. Figure 3c depicts the variation trend of σ_x for C–C HTMEE beam subjected to a different magnitude of hygrothermal loads.

Further, from Figure 3d, e, it can be witnessed that D_y and B_y has almost smooth variation along the beam length. It may be attributed to the fact that the pyro loads generated along the y -direction are almost constant. This may be because of the fact that the pyroelectric and pyromagnetic coefficients exist along the y -direction alone. The numerical evaluation is extended to analyze the independent effect of moisture concentration gradient Δm on the maximum values of the static parameters of C–C HTMEE beam. To this end, temperature rise ΔT is kept constant (100 K), while the humidity load or moisture concentration change Δm is varied. The results encapsulated in Table 2 suggest that the greater moisture concentration change (Δm) results in greater values of the x -direction displacement component U_x and y -direction displacement component U_y , whereas a marginal effect prevails on the transverse displacement component U_w . This may be a result of negligible amount of hygroscopic load $\{F_{hy}\}$ developed in z -direction in comparison with the thermal loads $\{F_{th}\}$ for the considered ΔT and Δm . From investigating the potentials of the system, it is witnessed that a mild influence of Δm exists on the electric potential ϕ . This may be attributed to the fact that the hygroscopic load developed has an insignificant influence on the electric potential of the system. In other words, the hygroscopic effect is minimal in comparison with the pyroloads generated due to the thermal effect. Analogously, due to direct effect of the electric potential, a minimal influence of the moisture concentration gradient Δm on the electric displacement components D_x , D_y , and D_z is witnessed.

Effect of empirical constants

The influence of temperature and moisture dependent elastic constants on the direct and derived quantities of C–C HTMEE beam has also been studied by varying the empirical constants (α^* and β^*) using the relation described as follows [37]:

$$C = C_0 (1 + \alpha^* \Delta T + \beta^* \Delta m) \quad (23)$$

in which, C is the temperature and moisture dependent elastic stiffness coefficient. Likewise, C_0 refers to the temperature and moisture independent elastic coefficient; α^* and β^* are the empirical constants related to temperature dependency and moisture dependency, respectively. The thermal load and hygroscopic load corresponding to a uniform temperature rise of 100 K and 2% moisture rise, respectively, is considered for the analysis. Since the effect of the temperature on the multiphysical

Table 2. Independent effect of moisture concentration gradient.

Static parameter (max. values)	Moisture concentration rise			
	$\Delta m = 0$	$\Delta m = 1$	$\Delta m = 5$	$\Delta m = 10$
$U_x (\times 10^{-3} \text{ m})$	−3.63	−3.65	−3.85	−4.04
$U_y (\times 10^{-3} \text{ m})$	0.393	0.401	0.436	0.479
$U_w (\times 10^{-3} \text{ m})$	0.41	0.415	0.42	0.43
$\phi (\times 10^7 \text{ V})$	1.6503	1.6633	1.6753	1.6803
$\psi (\text{A})$	−5.0663	−5.2629	−6.0496	−7.03
$\sigma_x (\text{GPa})$	3.4577	3.5029	3.6836	3.9096
$\sigma_y (\text{GPa})$	1.769	1.828	2.060	2.351
$\sigma_z (\text{GPa})$	1.853	1.885	2.011	2.169
$\tau_{xz} (\text{GPa})$	5.726	5.726	5.730	5.734
$\tau_{xy} (\text{GPa})$	−4.758	−4.370	−2.817	−0.876
$\tau_{yz} (\text{GPa})$	1.243	1.239	1.224	1.205
$D_x (\text{C m}^{-2})$	−5.61	−5.62	−5.64	−5.67
$D_y (\text{C m}^{-2})$	0.6938	0.6938	0.6937	0.6937
$D_z (\text{C m}^{-2})$	−3.9	−3.91	−3.95	−4.01
$B_x (\text{N Am}^{-1})$	9.403	10.251	13.640	17.875
$B_y (\text{N Am}^{-1})$	62.5323	62.5315	62.528	62.5237
$B_z (\text{N Am}^{-1})$	13.59	14.27	17.02	20.46

response is similar to that of the moisture concentration, the same values are taken for the empirical constants of temperature and moisture dependence [37]. The investigation concerning with the effect of empirical constants α^* and β^* on the direct quantities such as U_w , ϕ and ψ of C-C HTMEE beam is presented in Figure 4a–c, respectively. From these figures, it may be witnessed that the empirical constants $\alpha^* = \beta^* = -0.5$ exhibit a substantial effect on the direct quantities. This may be because of the empirical constants ranging from $-0.5 \leq \alpha \leq 0$, the elastic stiffness coefficients drastically changes which leads to the reduction in the stiffness $[K_{eq}]$ making the HTMEE beam more flexible. As a result, the overall $\left([K_{eq}]^{-1} \{F_{eq}\}\right)$ ratio remarkably increases. Further increase in absolute value of negative empirical constants ($\alpha^*, \beta^* = -0.5$), the elastic stiffness matrix $[K_{eq}]$ increases in such a way that the value $\left([K_{eq}]^{-1} \{F_{eq}\}\right)$ gradually reduces. Also, the predominant effect of negative empirical constants over positive empirical constants is noticed on the electric potential ϕ and magnetic potential ψ . However, from Figure 5a, it may be observed that with the increase in empirical constants, the normal stresses show an increasing trend, whereas shear stresses (τ_{xz} , τ_{xy} , and τ_{yz}) variation is significantly affected by $\alpha^* = \beta^* = -0.5$, as depicted in Figure 5b–d. On account of direct effects, the electric displacements and magnetic flux densities varies in a manner similar to that of the electric potential and magnetic potential, respectively. Therefore they are not illustrated here for the sake of brevity.

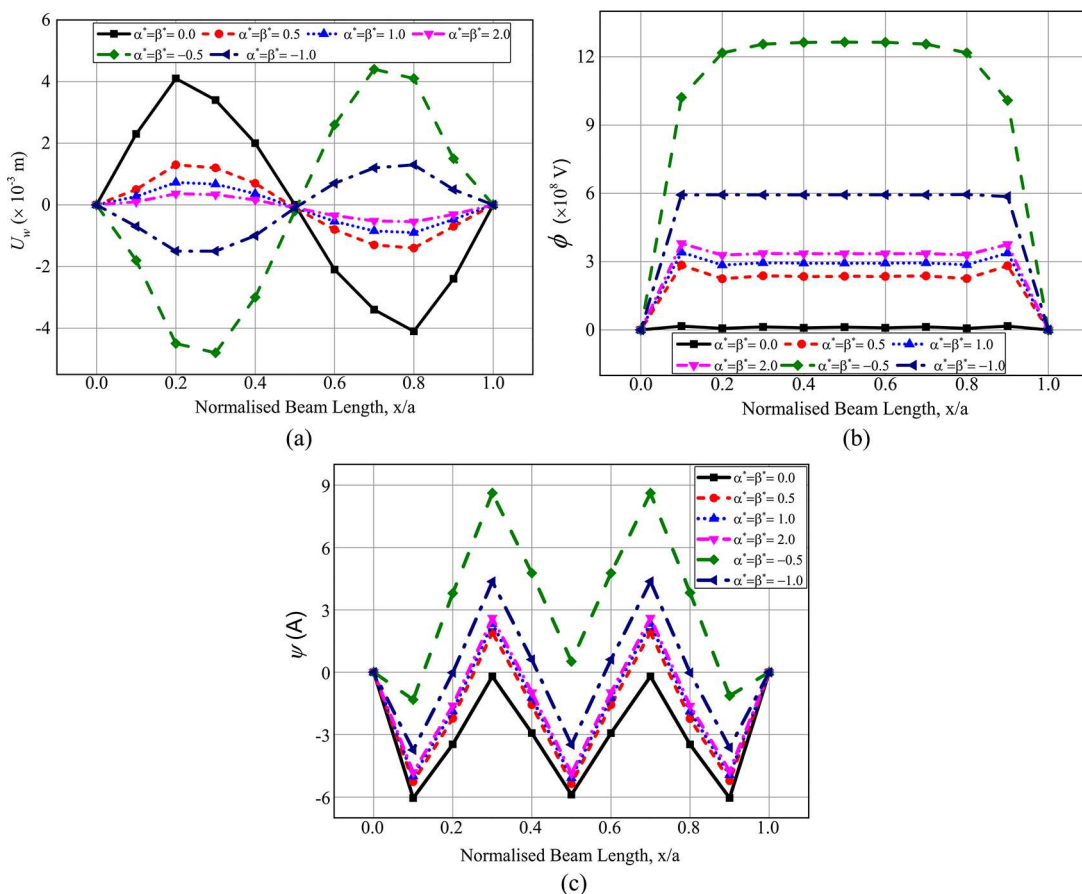


Figure 4. Effect of empirical constants on (a) z-direction displacement component U_w , (b) electric potential ϕ , and (c) magnetic potential ψ for C-C HTMEE beam. Note: HTMEE, hydro-thermo-magneto-electroelastic.

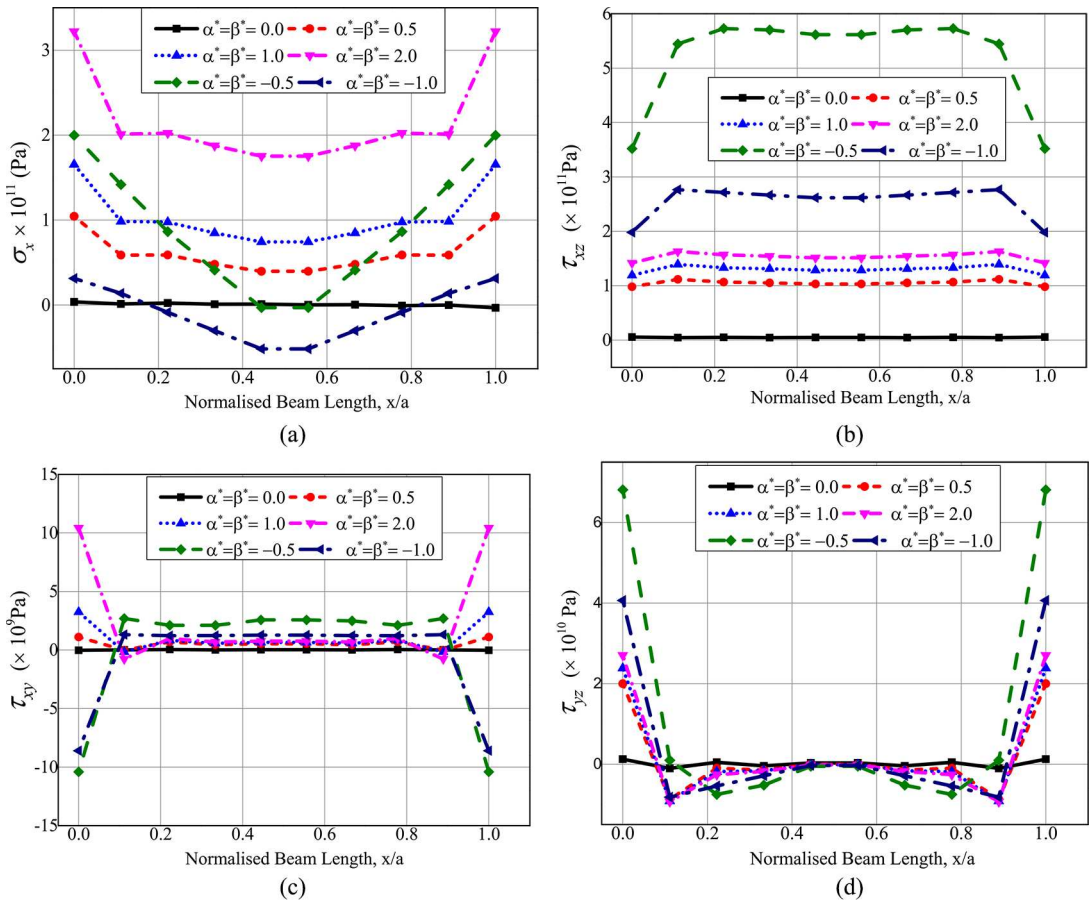


Figure 5. Effect of empirical constants on (a) normal stress σ_x , (b) shear stress τ_{xz} , (c) shear stress τ_{xy} , and (d) shear stress τ_{yz} for C-C HTMEE beam. Note: HTMEE, hydro-thermo-magneto-electroelastic.

Significant combination of empirical constant

The temperature and moisture fields behave differently for the varying temperature and moisture profiles, in contrast to uniform hygrothermal loads. Hence, evaluating the significant combination of empirical constants gains importance. The results presented in the previous section suggests that the empirical constants $\alpha^* = \beta^* = -0.5$ have a predominant influence on the static parameters. Therefore, the analysis is extended to investigate the effect of the different combination of β^* and α^* associated with constant values of $\alpha^* = -0.5$ and $\beta^* = -0.5$, respectively. In this regard, the most significant value of β^* in combination with α^* is evaluated through numerical analysis by keeping $\alpha^* = -0.5$ constant. Analogously, to predict the effect of α^* , and to determine the predominant value of α^* , the numerical calculations are performed by keeping $\beta^* = -0.5$ constant and varying α^* . From Table 3, it may be noticed that for the constant value of temperature dependency empirical constant $\alpha^* = -0.5$, a substantial effect of moisture dependency empirical constant $\beta^* = 2.0$ is observed on the direct quantities and derived quantities. Moreover, it is deduced that among the different values of α^* considered for the study, $\alpha^* = -0.5$ exhibits a significant influence on the static parameters when the moisture dependency empirical constant β^* is set to -0.5 . Meanwhile, for both the cases ($\alpha^* = -0.5$ and $\beta^* = -0.5$), the normal stress σ_x displays a maximum value for $\beta^* = 2.0$ and $\alpha^* = 2.0$ as demonstrated in Table 3.

Table 3. Significant combination of empirical constants.

	U_w (mm)	$(\times 10^7 \text{ V})$	ψ (kA)	σ_x (GPa)	σ_y (GPa)	σ_z (GPa)	τ_{xz} (GPa)	τ_{xy} (GPa)	τ_{yz} (GPa)	D_x ($\times 10^{-3} \text{ C m}^{-2}$)	D_y ($\times 10^{-3} \text{ C m}^{-2}$)	D_z ($\times 10^{-3} \text{ C m}^{-2}$)	B_x (N Am^{-1})	B_y (N Am^{-1})	B_z (N Am^{-1})	
β^*																
										$\alpha^* = -0.5$ (Constant)						
0	133.1	158.5	7.625	54.1	41.85	70.4	717.7	2.87	109.6	746.1	435.2	142.9	27.1	181.02	8.639	
0.5	167.3	190.5	9.63	70.6	57.7	73.8	862.4	3.73	124.6	849.8	534.5	172.9	32.34	229.2	8.88	
1.0	225.5	245.2	13.08	96.3	81.67	81.34	1112.5	5.07	148.3	1013.8	707.1	218.9	40.63	312.54	9.28	
2.0	756.1	790.4	47.04	265.9	241.4	164.5	3583.2	14.48	316.5	2176.9	241.2	658.5	99.22	1135.6	12.88	
-0.5	110.6	137.1	6.31	40.7	30.0	68.8	623.2	2.25	99.19	673.9	369.8	124.4	23.36	149.55	8.47	
-1.0	94.5	122.6	5.39	30.7	20.7	68.3	556.3	1.77	91.5	620.7	323.9	111.4	20.77	127.5	8.36	
α^*										$\beta^* = -0.5$ (Constant)						
0	46.1	2.84	4.17	3.78	3.02	2.5	9.25	0.09	2.471	21.5	64.88	28.2	11.22	60.6	7.6	
0.5	19.1	26.6	2.75	72.75	66.32	57.8	100.84	2.52	23.8	153.3	187.6	20.1	4.57	26.5	7.4	
1.0	12.23	32.67	2.37	130.1	120.97	109.12	129.2	4.58	29.44	190.7	339.8	25.7	5.11	16.5	7.52	
2.0	7.45	36.84	2.1	238.06	224.56	208.41	623.1	8.44	99.19	216.5	443.5	29.7	5.26	9.4	7.57	
-0.5	111.2	137.6	6.3	40.76	30.07	68.8	149.4	2.51	33.09	674.3	369.8	125.4	23.46	149.5	8.47	
-1.0	25.34	60.6	0.608	82.9	59.46	97.6	274.3	1.77	54.08	362.1	129.2	55.6	7.72	33.4	7.83	

Conclusion

This article makes the first attempt to explore the static behavior of HTMEE beams using the FE approach. The equilibrium equations of motion are derived using the minimum total potential energy principle and the coupled constitutive equations of HTMEE material accounting the linear coupling among the elastic, electric, hygroscopic, thermal, and magnetic fields. The condensation technique is exploited to solve the global FE equilibrium equations. Several numerical examples are considered to evaluate the effect of hygrothermal loads, moisture concentration gradient and boundary conditions on the direct quantities and derived quantities of HTMEE beams. It is observed that the greater magnitude of hygrothermal loads yield increased value of the static parameters. In addition, using the empirical constants, the effects of temperature and moisture dependent elastic stiffness coefficients are also examined. It is noticed that the empirical constants $\alpha^* = \beta^* = -0.5$ exhibit a significant influence on the static parameters except normal stresses, for which $\alpha^* = \beta^* = 2.0$ has a pronounced effect. Consequently, the present numerical examination reveals that a remarkable impact of hygrothermal loads, empirical constants and boundary conditions exists on the static performance of HTMEE beams. These results can set a benchmark for future analysis of HTMEE structures used in sensors, transducers, and micro-electromechanical systems.

Appendix A

The condensation method incorporated in computing the nodal displacement vectors is given as follows:

Considering Eq. (21) and solving for $\{\psi\}$,

$$\{\psi^e\} = [K_{\psi\psi}^e]^{-1} [K_{t\psi}^e]^T \{d_t^e\} - [K_{\psi\psi}^e]^{-1} [K_{\phi\psi}^e]^T \{\phi^e\} - [K_{\psi\psi}^e]^{-1} [\{F_{p,m}^e\} + \{F_{h,m}^e\}] \quad (\text{A.1})$$

Substituting Eq. (A.1) in Eq. (20), $\{\phi\}$ can be calculated as follows:

$$\begin{aligned} & [K_{t\phi}]^T \{d_t^e\} - [K_{\phi\phi}] \{\phi\} - [K_{\phi\psi}] \left[\begin{array}{l} [K_{\psi\psi}]^{-1} [K_{t\psi}]^T \{d_t\} - [K_{\psi\psi}]^{-1} [K_{\phi\psi}]^T \{\phi\} - \\ [K_{\psi\psi}]^{-1} (\{F_{p,m}\} + \{F_{h,m}\}) \end{array} \right] \\ & = (\{F_{p,e}\} + \{F_{h,e}\}) \\ & \{d_t\} - \left[[K_{t\phi}]^T - [K_{\phi\psi}^e] [K_{\psi\psi}]^{-1} [K_{t\psi}]^T \right] \{d_t\} - \{\phi\} \left[[K_{\phi\phi}] - [K_{\phi\psi}] [K_{\psi\psi}]^{-1} [K_{\phi\psi}]^T \right] \\ & + [K_{\phi\psi}] [K_{\psi\psi}]^{-1} (\{F_{p,m}\} + \{F_{h,m}\}) = \{F_{p,e}\} + \{F_{h,e}\} \end{aligned} \quad (\text{A.2})$$

$$[K_1] \{d_t\} - [K_2] \{\phi\} = (\{F_{p,e}\} + \{F_{h,e}\}) - [K_{\phi\psi}] [K_{\psi\psi}]^{-1} (\{F_{p,m}\} + \{F_{h,m}\})$$

$$[K_1] \{d_t\} - [K_2] \{\phi\} = \{F_{\phi_sol}\}$$

$$\{\phi\} = [K_2]^{-1} [K_1] \{d_t\} - [K_2]^{-1} \{F_{\phi_sol}\}$$

Meanwhile, Eqs. (A.1) and (A.2) are back substituted in Eq. (19) to compute the nodal displacements.

$$\begin{aligned} & [K_{tt}] \{d_t\} + [K_{t\phi}] \{\phi\} + [K_{t\psi}] \left[\begin{array}{l} [K_{\psi\psi}]^{-1} [K_{t\psi}]^T \{d_t\} - [K_{\psi\psi}]^{-1} [K_{\phi\psi}]^T \{\phi\} \\ - [K_{\psi\psi}]^{-1} [\{F_{p,m}\} + \{F_{h,m}\}] \end{array} \right] \\ & = \{F_{th}\} + \{F_{hy}\} \\ & \{d_t\} - \left[[K_{tt}] + [K_{t\psi}] [K_{\psi\psi}]^{-1} [K_{t\psi}]^T \right] \{d_t\} + \{\phi\} \left[[K_{t\phi}] - [K_{t\psi}] [K_{\psi\psi}]^{-1} [K_{\phi\psi}]^T \right] \\ & - [K_{t\psi}] [K_{\psi\psi}]^{-1} [\{F_{p,m}\} + \{F_{h,m}\}] = \{F_{th}\} + \{F_{hy}\} \end{aligned}$$

$$\begin{aligned}
 [K_5] \{d_t\} + [K_6] \{\phi\} - [K_{t\psi}] [K_{\psi\psi}]^{-1} [\{F_{p,m}\} + \{F_{h,m}\}] &= [\{F_{th}\} + \{F_{hy}\}] \\
 [K_5]_{-} \{d_t\} + [K_6] [[K_3] \{d_t\} - [K_2]^{-1} \{F_{\phi_sol}\}] - [K_{t\psi}] [K_{\psi\psi}]^{-1} [\{F_{p,m}\} + \{F_{h,m}\}] \\
 &= [\{F_{th}\} + \{F_{hy}\}] \\
 [[K_5] + [K_6] [K_3]] \{d_t\} - [K_6] [K_2]^{-1} [\{F_{p,e}\} + \{F_{h,e}\}] \\
 + [[K_6] [K_4] - [K_{t\psi}] [K_{\psi\psi}]^{-1}] [\{F_{p,m}\} + \{F_{h,m}\}] &= [\{F_{th}\} + \{F_{hy}\}] \\
 [K_7]_{-} \{d_t\} = [K_6] [K_2]^{-1} [\{F_{p,e}\} + \{F_{h,e}\}] \\
 + [[K_{t\psi}] [K_{\psi\psi}]^{-1} - [K_6] [K_4]] [\{F_{p,m}\} + \{F_{h,m}\}] + [\{F_{th}\} + \{F_{hy}\}] \\
 [K_7] \{d_t\} = [K_8] [\{F_{p,e}\} + \{F_{h,e}\}] + [K_9] [\{F_{p,m}\} + \{F_{h,m}\}] + [\{F_{th}\} + \{F_{hy}\}] \\
 [K_{eq}] \{d_t\} = \{F_{eq}\}
 \end{aligned} \tag{A.3}$$

The various stiffness and force vectors mentioned in Eqs. (A.1)–(A.3) can be explicitly represented as follows:

$$\begin{aligned}
 [K_1] &= [K_{\phi t}] - [K_{\psi\phi}] [K_{\psi\psi}]^{-1} [K_{\psi t}], \quad [K_2] = [K_{\phi\phi}] - [K_{\psi\phi}] [K_{\psi\psi}]^{-1} [K_{\phi\psi}], \quad [K_3] = [K_2]^{-1} [K_1] \\
 [K_4] &= [K_2]^{-1} [K_{\psi\phi}] [K_{\psi\psi}], \quad [K_5] = [K_{tt}] + [K_{t\psi}] [K_{\psi\psi}]^{-1} [K_{\psi t}] \\
 [K_6] &= [K_{t\phi}] - [K_{t\psi}] [K_{\psi\psi}]^{-1} [K_{\phi\psi}], \quad [K_7] = [K_5] + [K_6] [K_3], \quad [K_8] = [K_6] [K_2]^{-1} \\
 [K_9] &= [K_{t\psi}] [K_{\psi\psi}]^{-1} - [K_6] [K_4], \quad [K_{eq}] = [K_7], \quad [K_{1_psi}] = [K_{\psi t}] - [K_{\psi\phi}] [K_3] \\
 [K_{2_psi}] &= [K_{\psi\psi}]^{-1} [K_{\psi\phi}] [K_2]^{-1}, \quad [K_{3_psi}] = [K_{\psi\psi}]^{-1} [K_{\psi\phi}] [K_2]^{-1} [K_{\psi\phi}]^T [K_{\psi\psi}]^{-1} + [K_{\psi\psi}]^{-1} \\
 \{F_{eq}\} &= [K_9] [\{F_{p,m}\} + \{F_{h,m}\}] + [K_8] [\{F_{p,e}\} + \{F_{h,e}\}] + [\{F_{th}\} + \{F_{hy}\}] \\
 \{F_{\phi_sol}\} &= [\{F_{p,e}\} + \{F_{h,e}\}] - [K_{\psi\phi}]^T [K_{\psi\psi}]^{-1} [\{F_{p,m}\} + \{F_{h,m}\}]
 \end{aligned} \tag{A.4}$$

ORCID

Subhas Chandra Kattimani  <http://orcid.org/0000-0002-2477-3783>

References

- [1] W. Smittakorn and P. R. Heyliger, “An Adaptive Wood Composite: Theory,” *Wood Fib. Sci.*, vol. 33, no. 4, pp. 595–608, 2001.
- [2] W. Smittakorn and P. R. Heyliger, “Adaptive Wood Composite: Experiment,” *J. Struct. Eng.*, vol. 129, pp. 699–702, 2003. DOI: [10.1061/\(asce\)0733-9445\(2003\)129:5\(699\)](https://doi.org/10.1061/(asce)0733-9445(2003)129:5(699)).
- [3] F. Ebrahimi and M. R. Barati, “Hygrothermal Buckling Analysis of Magnetically Actuated Embedded Higher Order Functionally Graded Nanoscale Beams Considering the Neutral Surface Position,” *J. Therm. Stresses*, vol. 39, no. 10, pp. 1210–1229, 2016. DOI: [10.1080/01495739.2016.1215726](https://doi.org/10.1080/01495739.2016.1215726).
- [4] W. Chen and T. Shioya, “Piezothermoelastic Behavior of a Pyroelectric Spherical Shell,” *J. Therm. Stresses*, vol. 24, no. 2, pp. 105–120, 2001. DOI: [10.1080/01495730150500424](https://doi.org/10.1080/01495730150500424).

- [5] M. Saadatfar and M. Aghaie-Khafri, "On the Behavior of a Rotating Functionally Graded Hybrid Cylindrical Shell with Imperfect Bonding Subjected to Hygrothermal Condition," *J. Therm. Stresses*, vol. 38, no. 8, pp. 854–881, 2015. DOI: [10.1080/01495739.2015.1038487](https://doi.org/10.1080/01495739.2015.1038487).
- [6] W. Smittakorn and P. R. Heyliger, "A Discrete-layer Model of Laminated Hygro-thermopiezoelectric Plates," *Mech. Compos. Mater. Struct.*, vol. 7, pp. 79–104, 2000. DOI: [10.1080/107594100305438](https://doi.org/10.1080/107594100305438).
- [7] A. M. Zenkour, "Hygro-thermoelastic Responses of Inhomogeneous Piezoelectric and Exponentially Graded Cylinders," *Int. J. Pres. Ves. Pip.*, vol. 119, pp. 8–18, 2014. DOI: [10.1016/j.ijpvp.2014.02.001](https://doi.org/10.1016/j.ijpvp.2014.02.001).
- [8] S. B. Kerur and A. Ghosh, "Geometrically Non-linear Bending Analysis of Piezoelectric Fiber-reinforced Composite (MFC/AFC) Cross-ply Plate Under Hygrothermal Environment," *J. Therm. Stresses*, vol. 36, no. 12, pp. 1255–1282, 2013. DOI: [10.1080/01495739.2013.818887](https://doi.org/10.1080/01495739.2013.818887).
- [9] G. Altay and M. C. Dokmeci, "Some Hamiltonian-type Variational Principles for Motions of a Hygro-thermoelastic Medium," *J. Therm. Stresses*, vol. 23, pp. 273–284, 2000. DOI: [10.1080/014957300280443](https://doi.org/10.1080/014957300280443).
- [10] E. Pan, "Exact Solution for Simply Supported and Multilayered Magneto-Electro-Elastic Plates," *J. Appl. Mech.*, vol. 68, pp. 608–618, 2001. DOI: [10.1115/1.1380385](https://doi.org/10.1115/1.1380385).
- [11] F. Ramirez, P. R. Heyliger, and E. Pan, "Free Vibration Response of Two-dimensional Magneto-electro-Elastic Laminated Plates," *J. Sound Vib.*, vol. 292, pp. 626–644, 2006. DOI: [10.1016/j.jsv.2005.08.004](https://doi.org/10.1016/j.jsv.2005.08.004).
- [12] J. Chen, H. Chen, E. Pan, and P. R. Heyliger, "Modal Analysis of Magneto-electro-elastic Plates using the State-vector Approach," *J. Sound Vib.*, vol. 304, pp. 722–734, 2007. DOI: [10.1016/j.jsv.2007.03.021](https://doi.org/10.1016/j.jsv.2007.03.021).
- [13] Y. Wang, R. Xu, H. Ding, and J. Chen, "Three Dimensional Exact Solutions for Free Vibrations of Simply Supported Magneto-electro-elastic Cylindrical Panels," *Int. J. Eng. Sci.*, vol. 48, pp. 1778–1796, 2010. DOI: [10.1016/j.ijengsci.2010.09.022](https://doi.org/10.1016/j.ijengsci.2010.09.022).
- [14] L. Xin and Z. Hu, "Free Vibration of Simply Supported and Multilayered Magneto-Electro-Elastic Plates," *Compos. Struct.*, vol. 121, pp. 344–350, 2015. DOI: [10.1016/j.compstruct.2014.11.030](https://doi.org/10.1016/j.compstruct.2014.11.030).
- [15] R. G. Lage, C. M. M. Soares, C. A. M. Soares, and J. N. Reddy, "Layerwise Partial Mixed Finite Element Analysis of Magneto-Electro-Elastic Plates," *Comput. Struct.*, vol. 82, pp. 1293–1301, 2004. DOI: [10.1016/j.compstruc.2004.03.026](https://doi.org/10.1016/j.compstruc.2004.03.026).
- [16] E. Pan and F. Han, "Exact Solutions for Functionally Graded and Layered Magneto-Electro-Elastic Plates," *Int. J. Eng. Sci.*, vol. 43, pp. 321–339, 2005. DOI: [10.1016/j.ijengsci.2004.09.006](https://doi.org/10.1016/j.ijengsci.2004.09.006).
- [17] R. K. Bhargale and N. Ganesan, "Static Analysis of Simply Supported Functionally Graded and Layered Magneto-Electro-Elastic Plates," *Int. J. Solids Struct.*, vol. 43, no. 10, pp. 3230–3253, 2006. DOI: [10.1016/j.ijsolstr.2005.05.030](https://doi.org/10.1016/j.ijsolstr.2005.05.030).
- [18] D. J. Huang, H. J. Ding, and W. Q. Chen, "Analytical Solution for Functionally Graded Magneto-Electro-Elastic Plane Beams," *Int. J. Eng. Sci.*, vol. 45, pp. 467–485, 2007. DOI: [10.1016/j.ijengsci.2007.03.005](https://doi.org/10.1016/j.ijengsci.2007.03.005).
- [19] A. Alaimo, I. Benedetti, and A. Milazzo, "A Finite Element Formulation for Large Deflection of Multilayered Magneto-Electro-Elastic Plates," *Compos. Struct.*, vol. 107, pp. 643–653, 2014. DOI: [10.1016/j.compstruct.2013.08.032](https://doi.org/10.1016/j.compstruct.2013.08.032).
- [20] Y. S. Li, "Buckling Analysis of Magneto-electroelastic Plate Resting on Pasternak Elastic Foundation," *Mech. Res. Commun.*, vol. 56, pp. 104–114, 2014. DOI: [10.1016/j.mechrescom.2013.12.007](https://doi.org/10.1016/j.mechrescom.2013.12.007).
- [21] Z. Lang and L. Xuewu, "Buckling and Vibration Analysis of Functionally Graded Magneto-Electro-Thermo-Elastic Circular Cylindrical Shells," *Appl. Math. Model.*, vol. 37, pp. 2279–2292, 2013. DOI: [10.1016/j.apm.2012.05.023](https://doi.org/10.1016/j.apm.2012.05.023).
- [22] S. C. Kattimani and M. C. Ray, "Smart Damping of Geometrically Nonlinear Vibrations of Magneto-Electro-Elastic Plates," *Compos. Struct.*, vol. 14, pp. 51–63, 2014. DOI: [10.1016/j.compstruct.2014.03.050](https://doi.org/10.1016/j.compstruct.2014.03.050).
- [23] S. C. Kattimani and M. C. Ray, "Control of Geometrically Nonlinear Vibrations of Functionally Graded Magneto-Electro-Elastic Plates," *Int. J. Mech. Sci.*, vol. 99, pp. 154–167, 2015. DOI: [10.1016/j.ijmecsci.2015.05.012](https://doi.org/10.1016/j.ijmecsci.2015.05.012).
- [24] S. C. Kattimani and M. C. Ray, "Active Control of Large Amplitude Vibrations of Smart Magneto-Electro-Elastic Doubly Curved Shells," *Int. J. Mech. Mater. Des.*, vol. 10, no. 4, pp. 351–378, 2014. DOI: [10.1007/s10999-014-9252-3](https://doi.org/10.1007/s10999-014-9252-3).
- [25] M. Sunar, A. Z. Al-Garni, M. H. Ali, and R. Kahraman, "Finite Element Modeling of Thermopiezomagnetic Smart Structures," *AIAA J.*, vol. 40, pp. 1845–1851, 2002. DOI: [10.2514/2.1862](https://doi.org/10.2514/2.1862).
- [26] Y. Ootao and Y. Tanigawa, "Transient Analysis of Multilayered Magneto-Electro-Thermoelastic Strip due to Nonuniform Heat Supply," *Compos. Struct.*, vol. 68, pp. 471–480, 2005. DOI: [10.1016/j.compstruct.2004.04.013](https://doi.org/10.1016/j.compstruct.2004.04.013).
- [27] A. Kumaravel, N. Ganesan, and R. Sethuraman, "Steady-State Analysis of a Three-Layered Electro-Magneto-Elastic Strip in a Thermal Environment," *Smart Mater. Struct.*, vol. 16, pp. 282–295, 2007. DOI: [10.1088/0964-1726/16/2/006](https://doi.org/10.1088/0964-1726/16/2/006).
- [28] A. Kumaravel, N. Ganesan, and R. Sethuraman, "Buckling and Vibration Analysis of Layered and Multiphase Magneto-electroelastic Cylinders Subjected to Uniform Thermal Loading," *Multidiscip. Model. Mater. Struct.*, vol. 6, no. 4, pp. 475–492, 2010. DOI: [10.1108/15736101011095145](https://doi.org/10.1108/15736101011095145).
- [29] P. Kondaiah, K. Shankar, and N. Ganesan, "Studies on Magneto-Electro-Elastic Cantilever Beam Under Thermal Environment," *Coupled Syst. Mech.*, vol. 1, no. 2, pp. 205–217, 2012. DOI: [10.12989/csm.2012.1.2.205](https://doi.org/10.12989/csm.2012.1.2.205).
- [30] P. Kondaiah, K. Shankar, and N. Ganesan, "Pyroelectric and Pyromagnetic Effects on Behaviour of Magneto-Electro-Elastic Plate," *Coupled Syst. Mech.*, vol. 2, pp. 1–22, 2013. DOI: [10.12989/csm.2013.2.1.001](https://doi.org/10.12989/csm.2013.2.1.001).
- [31] M. Vinyas and S. C. Kattimani, "Static Studies of Stepped Functionally Graded Magneto-Electro-Elastic Beam Subjected to Different Thermal Loads," *Compos. Struct.*, vol. 163, pp. 216–237, 2017. DOI: [10.1016/j.compstruct.2016.12.040](https://doi.org/10.1016/j.compstruct.2016.12.040).

- [32] M. Vinyas and S. C. Kattimani, "A Finite Element based Assessment of Static Behavior of Multiphase Magneto-Electro-Elastic Beams Under Different Thermal Loading," *Struct. Eng. Mech.* vol. 62, no. 5, pp. 519–535, 2017.
- [33] M. Vinyas and S. C. Kattimani, "Static Analysis of Stepped Functionally Graded Magneto-Electro-Elastic Plates in Thermal Environment: A Finite Element Study," *Compos. Struct.*, vol. 178, pp. 63–85, 2017. DOI: [10.1016/j.compstruct.2017.06.068](https://doi.org/10.1016/j.compstruct.2017.06.068).
- [34] M. Vinyas and S. C. Kattimani, "Hygrothermal Analysis of Magneto-Electro-Elastic Plate using 3D Finite Element Analysis," *Compos. Struct.*, vol. 180, pp. 617–637, 2017. DOI: [10.1016/j.compstruct.2017.08.015](https://doi.org/10.1016/j.compstruct.2017.08.015).
- [35] M. Vinyas and S. C. Kattimani, "Influence of Coupled Fields on Free Vibration and Static Behavior of Functionally Graded Magneto-Electro-Thermo-Elastic Plate," *J. Intell. Mater. Syst. Struct.*, 2017. DOI: [10.1177/1045389X17740739](https://doi.org/10.1177/1045389X17740739).
- [36] M. Vinyas and S. C. Kattimani, "Investigation of the Effect of BaTiO₃/CoFe₂O₄ Particle Arrangement on the Static Response of Magneto-Electro-Thermo-Elastic Plates," *Compos. Struct.*, vol. 185, pp. 51–64, 2018. DOI: [10.1016/j.compstruct.2017.10.073](https://doi.org/10.1016/j.compstruct.2017.10.073).
- [37] A. H. Akbarzadeh and Z. T. Chen, "Magneto-electroelastic Behavior of Rotating Cylinders Resting on an Elastic Foundation Under Hygrothermal Loading," *Smart Mater. Struct.*, vol. 2, pp. 125013, 2012. DOI: [10.1088/0964-1726/21/12/125013](https://doi.org/10.1088/0964-1726/21/12/125013).
- [38] A. H. Akbarzadeh and Z. T. Chen, "Hygrothermal Stresses in One Dimensional Functionally Graded Piezoelectric Media in Constant Magnetic Field," *Compos. Struct.*, vol. 97, pp. 317–331, 2013. DOI: [10.1016/j.compstruct.2012.09.058](https://doi.org/10.1016/j.compstruct.2012.09.058).
- [39] A. H. Akbarzadeh and D. Pasini, "Multiphysics of Multilayered and Functionally Graded Cylinders under Prescribed Hygro-thermomagneto-electromechanical Loading," *J. Appl. Mech. T. ASME*, vol. 81, pp. 041018, 2014. DOI: [10.1115/1.4025529](https://doi.org/10.1115/1.4025529).
- [40] M. Saadatfar and A. M. Khafri, "Hygro-thermomagneto-electroelastic Analysis of a Functionally Graded Magneto-electroelastic Hollow Sphere Resting on an Elastic Foundation," *Smart Mater. Struct.*, vol. 23, pp. 035004, 2014. DOI: [10.1088/0964-1726/23/3/035004](https://doi.org/10.1088/0964-1726/23/3/035004).